Stellar and dust emission profiles of IMEGIN galaxies

A. Nersesian[1], R. Adam[2], P. Ade[3], H. Ajeddig[4], P. André[4], E. Artis[5,6], H. Aussel[4], M. Baes[1], A. Beelen[7], A. Benoît[8], S. Berta[9], L. Bing[7], O. Bourrion[5], M. Calvo[8], A. Catalano[5], M. De Petris[10], F.-X. Désert[11], S. Doyle[3], E. F. C. Driessen[9], G. Ejlali[12], A. Gomez[13], J. Goupy[8], C. Hanser[5], S. Katsioli[14,15], F. Kéruzoré[16], C. Kramer[9], B. Ladjelate[17], G. Lagache[7], S. Leclercq[9], J.-F. Lestrade[18], J. F. Macías-Pérez[5], S. C. Madden[4], A. Maury[4], P. Mauskopf[3,19], F. Mayet[5], A. Monfardini[8], A. Moyer-Anin[5], M. Muñoz-Echeverría[5], L. Pantoni[4,20], L. Perotto[5], G. Pisano[10], N. Ponthieu[11], V. Revéret[4], A. J. Rigby[21], A. Ritacco[22,23], C. Romero[24], H. Roussel[25], F. Ruppin[26], K. Schuster[9], A. Sievers[17], C. Tucker[3], E. M. Xilouris[14], and R. Zylka[9]

[1]Sterrenkundig Observatorium Universiteit Gent, B-9000 Gent, Belgium
[2]Université Côte d'Azur, Observatoire de la Côte d'Azur, CNRS, Laboratoire Lagrange, France
[3]School of Physics and Astronomy, Cardiff University, CF24 3AA, UK
[4]Université Paris-Saclay, Université Paris Cité, CEA, CNRS, AIM, 91191 Gif-sur-Yvette, France
[5]Université Grenoble Alpes, CNRS, Grenoble INP, LPSC-IN2P3, 38000 Grenoble, France
[6]Max Planck Institute for Extraterrestrial Physics, 85748 Garching, Germany
[7]Aix Marseille Univ, CNRS, CNES, LAM, Marseille, France
[8]Université Grenoble Alpes, CNRS, Institut Néel, France
[9]Institut de RadioAstronomie Millimétrique (IRAM), Grenoble, France
[10]Dipartimento di Fisica, Sapienza Università di Roma, I-00185 Roma, Italy
[11]Univ. Grenoble Alpes, CNRS, IPAG, 38000 Grenoble, France
[12]Institute for Research in Fundamental Sciences (IPM), Larak Garden, 19395-5531 Tehran, Iran
[13]Centro de Astrobiología (CSIC-INTA), Torrejón de Ardoz, 28850 Madrid, Spain
[14]National Observatory of Athens, IAASARS, GR-15236 Athens, Greece
[15]Faculty of Physics, University of Athens, GR-15784 Zografos, Athens, Greece
[16]High Energy Physics Division, Argonne National Laboratory, Lemont, IL 60439, USA
[17]Instituto de Radioastronomía Milimétrica (IRAM), Granada, Spain
[18]LERMA, Observatoire de Paris, PSL Research Univ., CNRS, Sorbonne Univ., UPMC, 75014 Paris, France
[19]School of Earth & Space and Department of Physics, Arizona State University, AZ 85287, USA
[20]Université Paris-Saclay, CNRS, Institut d'astrophysique spatiale, 91405 Orsay, France
[21]School of Physics and Astronomy, University of Leeds, Leeds LS2 9JT, UK
[22]INAF-Osservatorio Astronomico di Cagliari, 09047 Selargius, Italy
[23]Laboratoire de Physique de l'École Normale Supérieure, ENS, PSL, CNRS, Sorbonne Université, Université de Paris, 75005 Paris, France
[24]Department of Physics and Astronomy, University of Pennsylvania, PA 19104, USA
[25]Institut d'Astrophysique de Paris, CNRS (UMR7095), 75014 Paris, France
[26]University of Lyon, UCB Lyon 1, CNRS/IN2P3, IP2I, 69622 Villeurbanne, France

Abstract. We present a morphological analysis of a set of spiral galaxies from the NIKA2 Guaranteed Time Large Program, IMEGIN. We have fitted a single Sérsic model on a set of broadband images, from ultra-violet (UV) to millimeter (mm) wavelengths, using the modelling code `Statmorph`. With the recently

acquired NIKA2 1.15- and 2-mm observations, it is possible to extend such a morphological analysis to the mm regime and investigate the two-dimensional (2D) distribution (exponential, Gaussian) of the very cold dust (<15 K). We show preliminary results of the 2D large-scale distribution of stars and dust in spiral galaxies, how they relate to each other, and highlight how they differ from galaxy to galaxy.

1 Introduction

Morphology is a key aspect used to understand galaxies, shedding light on their history and evolution. Numerous studies have demonstrated a strong correlation of galaxy morphology with quantities like optical colors, star-formation rate (SFR), and stellar mass [e.g. 1–4]. Visual inspection remains the primary way to classify galaxies, typically grouping them into ellipticals, lenticulars, spirals, and irregulars [5].

A more quantitative approach to describe the morphology of a galaxy and its internal structure is by fitting the surface brightness distribution with a general Sérsic profile [6]. Three of the main free parameters of a two-dimensional (2D) Sérsic profile are: the Sérsic index n, the effective size enclosing half of the light within a galaxy (R_e), and the effective surface brightness (μ_e). Other important free parameters, which are included in the 2D profile fitting, are the ellipticity and orientation of the elliptical isophotes. Different values of the Sérsic index can be used to characterise the brightness profile of stellar and dust distributions in galaxies. For example, a Sérsic index $n = 0.5$ returns a Gaussian profile, $n = 1$ describes an exponential law, while $n = 4$ gives a de Vaucouleurs profile.

Another important aspect of quantifying galaxy structure is its dependence on the observed wavelength. Many studies have shown the wavelength dependence of galaxy morphology by fitting 2D Sérsic profiles in ultra-violet (UV), optical, and near-infrared (NIR) broad-band images [e.g. 7–11]. For example, the structural parameters of elliptical galaxies have a smooth transition with wavelength. On the other hand, the structure of spiral galaxies has a more complex dependence with wavelength caused by stellar population age and metallicity gradients, as well as dust attenuation effects that exist in those systems [e.g. 12, 13]. [14] performed a similar morphology study on a sample of nearby galaxies, by fitting 2D Sérsic profiles, but in the mid-infrared (MIR) and far-infrared (FIR). The authors reported an increase in the R_e of the dust with increasing FIR wavelengths. They also reported a flat dependence of the Sérsic index n with wavelength, taking a value systematically below 1 in all *Herschel* bands. Such a morphological analysis is important when modelling the three-dimensional (3D) structure of the various disc components (e.g., stellar and dust) of spiral galaxies with radiative transfer (RT). A common assumption in a RT model is to represent the dust surface density with an exponential model [e.g., 15–19], similar to the stellar disc. It is quite rare for a non-exponential model to be used for the dust disc in RT modelling [14].

In this work, we want to investigate whether or not the morphological trends found by [14] in the FIR bands continue in the millimetre (mm) regime. We will use newly obtained mm maps of 9 nearby spiral galaxies. These new observations are part of IMEGIN (Interpreting the Millimetre Emission of Galaxies with IRAM and NIKA2; PI: S. Madden), a Guaranteed Time Large program of 200 hours targeting nearby galaxies at a distance of less than 25 Mpc. Dedicated studies on the mm maps of individual galaxies are presented in upcoming papers, NGC 891 [20], NGC 2146 and NGC 2976 [21], and NGC 4254 [22]. For the purpose of our analysis, we have also collected archival data that cover the full spectral range from UV-submm. In that way, we will consistently measure the stellar and dust profiles of those 9 galaxies and perform a panchromatic morphological analysis similar to the study by [23].

2 Observations with NIKA2 and ancillary data
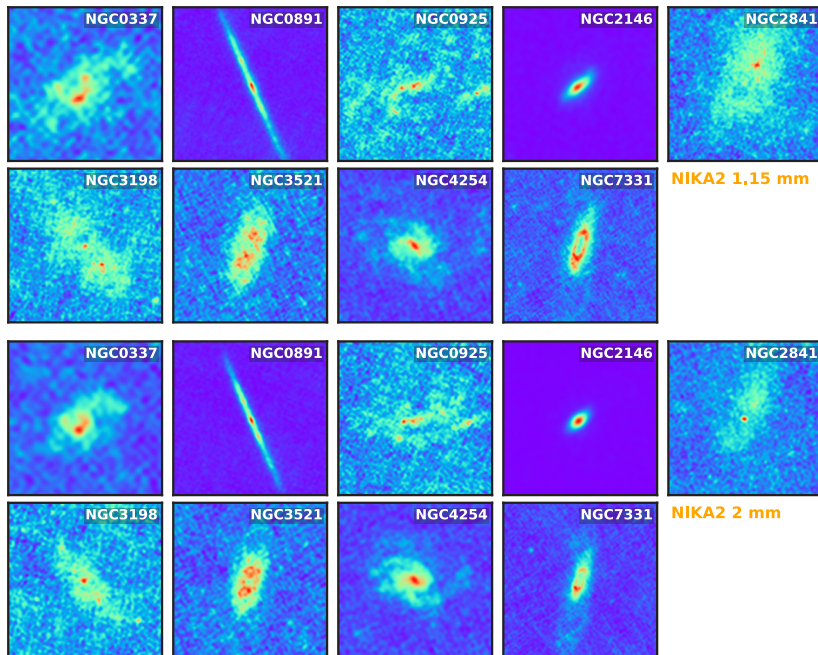
Figure 1. NIKA2 high-resolution millimetre observations of nine nearby spiral galaxies at 1.15 mm (top) and 2 mm (bottom). The maps are presented in their native resolution of 11.1" and 17.6", respectively.

The mm observations of IMEGIN were carried out between October 2019 and January 2023, using the NIKA2 [24–26] camera on the IRAM 30-m Telescope. The maps of each galaxy at 1.15 mm and 2 mm were reduced using the `piic/gildas` software [27, 28] and are shown in Fig. 1. In addition, for all the galaxies in this work, we used data available in the DustPedia [29] archive[1]. These datasets are a combination of images observed from ground-based and space telescopes. In particular, we use images observed with GALEX, SDSS, 2MASS, WISE, and *Herschel*, covering a broad wavelength range from the UV to the submm wavelength domain.

3 Method of analysis

We pre-processed all images using an automatic procedure as was developed by Pantoni et al. (2024, in prep.) [22]. First, foreground stars were identified from the 2MASS All-Sky Catalog of Point Sources, and removed from the GALEX, SDSS, 2MASS, and WISE images. Then, all images were corrected for background and foreground emission. The final steps in our image processing pipeline were, 1) convolving all images to the SPIRE 500 μm point-spread function (PSF) using the convolution kernels of [30], and 2) re-gridding them on the same spatial resolution of 12". We also generated uncertainty maps through a boot-strapping Monte Carlo method [22]. We used the `python` package `StatMorph` [31] to fit 2D

---

[1]http://dustpedia.astro.noa.gr

Sérsic models on the individual galaxy images. The uncertainty maps of each photometric band were considered in the fitting. By applying `StatMorph` on each map, we were able to recover the main morphological parameters (Sérsic index n, R_e) of each galaxy at different wavelengths. That allowed us to quantify how the morphological structure of a galaxy evolves as a function of wavelength.

4 Results

In this section, we present the results of our analysis. In Fig. 2 we show the wavelength dependence of the Sérsic index n (top panel) and half-light radius R_e (bottom panel) for the nine spiral galaxies. The half-light radius R_e is normalised by $R_{e,W1}$, the effective size measured in the WISE 1 band representative of the stellar disc structure. Focusing on the Sérsic index, we find that in the UV regime on average the Sérsic index is below 1, then rises above one in the optical and NIR, and then drops below 1 and remains flat in the MIR, FIR and mm regime.

Looking at the galaxy sizes, we retrieve the expected behaviour where galaxies appear more extended in the UV, followed by a decline in size in the optical /NIR. This behaviour is expected and can be explained as the mix of two effects: the intrinsic age and metallicity gradients of the stellar populations, and dust attenuation at short wavelengths [e.g. 8, 10, 12]. At the MIR regime we notice a flat size–wavelength dependence, and then in FIR we notice a steady increase as it has been reported before in the literature [14, 23].

5 Discussion

In this section, we focus on the FIR/mm regime. The main goal of this analysis is to investigate if the morphological trends of the dust component, which were reported by [14] in the FIR, continue in the mm regime. In Fig. 3, we show again the wavelength dependence of the Sérsic index n (top panel) and half-light radius R_e (bottom panel) for the nine spiral galaxies, but focusing on, only in the FIR/mm regime. We see that our results in the FIR are in excellent agreement with the median trends shown in [14], for both n and $R_e/R_{e,W1}$. However, we
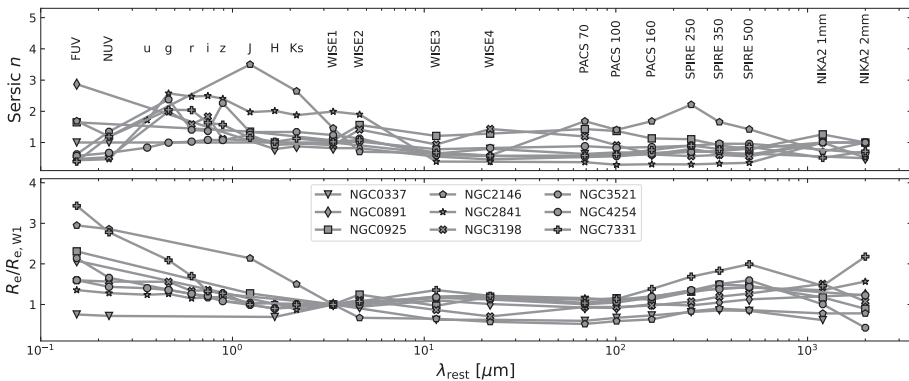
Figure 2. Morphological parameters of nine spiral galaxies as a function of wavelength. Top: Sérsic index n. Bottom: Effective galaxy size R_e normalised by $R_{e,W1}$ (see text). Different markers are given for each galaxy (see legend).

find that in the mm the emission is no longer described by a Gaussian profile ($n = 0.5$) but instead is described by an exponential profile ($n = 1$). This means that on average the mm luminosity is stronger in the central region of the galaxies. We also find that galaxies appear smaller in size at mm wavelengths compared to the FIR.
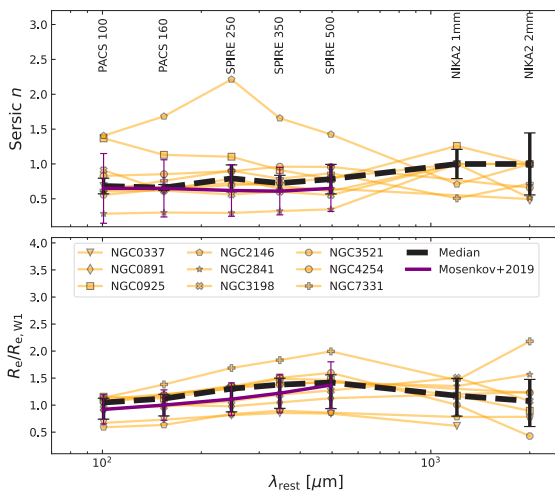
Figure 3. Morphological parameters of nine spiral galaxies as a function of FIR and mm wavelengths. Top: Sérsic index n. Bottom: Effective galaxy size R_e normalised by $R_{e,W1}$ (see text). Different markers are given for each galaxy (see legend). The black dashed lines and black errorbars show the median trends and standard deviation at each waveband, respectively. The purple lines show the median trends of [14].

We speculate two potential reasons for those trends. Either the mm emission has a significant contribution from the radio continuum (i.e. free-free and synchrotron emissions) powered by stellar evolution in the disc and at the centre of those galaxies. It is well-established that a tight correlation exists between radio continuum emission and star-formation rate [e.g., 32, 33]. So we get more radio continuum emission in the arms, which may extend to the outer disc of spiral galaxies. Thus, in the mm we start tracing the stellar disc again. Another possible explanation of our results is that we only detect the very cold dust in the central regions of the galaxies (<15 K) and miss the extended dust emission in the outskirts due to lower sensitivity of the instrument at these wavelengths. Further analysis, observations, and uncertainty estimations on the retrieved morphological parameters are needed to conclude which scenario is true.

6 Conclusions

We derived structural parameters for the IMEGIN galaxies based on multi-wavelength images (UV-mm). These parameters are the Sérsic index (galaxy morphology) and the effective radius (galaxy size). Based on the Sérsic index, the surface brightness of the stellar disc in our galaxies is close to an exponential profile. At 100–500 μm, the dust emission resembles a Gaussian profile. At 1.15 mm and 2 mm, the emission is distributed by an exponential profile. The R_e of the dust profile steadily increases with wavelength up to 500 μm and declines at the mm regime.

Two possible explanations for the trends we find at FIR and mm wavelengths are: 1) the mm emission is powered by non-thermal emission (i.e. synchrotron) caused by stellar evolution in the disc and at the centre of those galaxies, thus in the mm we start tracing again the stellar disc, 2) the NIKA2 observations detect the very cold dust in the central regions of the galaxies (<15 K) and miss the extended dust emission in the outskirts due to the instrument's lower sensitivity at these wavelengths.

Acknowledgements

References

[1] Jr. R. C. Kennicutt, ARA&A **36**, 189 (1998)

[2] I. Strateva, *et al.*, AJ **122**, 1861 (2001)

[3] A. Schawinski, *et al.*, MNRAS **440**, 889 (2014)

[4] A. Nersesian, *et al.*, A&A **624**, 80 (2019)

[5] G. de Vaucouleurs, Handbuch der Physik **53**, 275 (1959)

[6] J. L. Sérsic, Boletin AAA **6**, 41 (1963)

[7] F. La Barbera, *et al.*, MNRAS **408**, 1313 (2010)

[8] L. S. Kelvin, *et al.*, MNRAS **421**, 1007 (2012)

[9] B. Häußler, *et al.*, MNRAS **430**, 330 (2013)

[10] B. Vulcani, *et al.*, MNRAS **441**, 1340 (2014)

[11] E. -D. Paspaliaris, *et al.*, A&A **669**, A11 (2023)

[12] A. Nersesian, *et al.*, A&A **673**, A63 (2023)

[13] M. Baes, *et al.*, A&A, in prep. (2023)

[14] A. V. Mosenkov, *et al.*, A&A **622**, 132 (2019)

[15] I. De Looze, *et al.*, A&A **571**, A69 (2014)

[16] S. Verstocken, *et al.*, A&A **637**, A24 (2020)

[17] A. Nersesian, *et al.*, A&A **637**, A25 (2020)

[18] A. Nersesian, *et al.*, A&A **643**, A90 (2020)

[19] S. Viaene, *et al.*, A&A **638**, A150 (2020)

[20] S. Katsioli, *et al.*, A&A **679**, A7 (2023)

[21] G. Ejlali, *et al.*, A&A, in preparation (2023)

[22] L. Pantoni, *et al.*, A&A, in preparation (2024)

[23] M. Baes, *et al.*, A&A **641**, 119 (2020)

[24] M. Calvo, *et al.*, Journal of Low Temperature Physics **184**, 816 (2016)

[25] O. Bourrion, *et al.*, Journal of Instrumentation **11**, P11001 (2016)

[26] R. Adam, *et al.*, A&A **609**, A115 (2018)

[27] R. Zylka, MOPSIC: Extended Version of MOPSI (2013)

[28] S. Berta & R. Zylka, IRAM report (2022)

[29] J.J. Davies, *et al.*, PASP **129**, 044102 (2017)

[30] G. Aniano, *et al.*, PASP **123**, 1218 (2011)

[31] V. Rodriguez-Gomez, *et al.*, MNRAS **483**, 4140 (2019)

[32] A. Boselli, *et al.*, A&A **579**, A102 (2015)

[33] D. J. B. Smith, *et al.*, A&A **648**, A6 (2021)